

A Simple Fracture Mechanics Method for Measuring the Interfacial Toughness with Microbond Tests

J. A. Nairn* and R. J. Scheer†

*Material Science & Engineering, University of Utah, Salt Lake City, Utah 84112, USA

†Protein Solutions, Inc., 350 West 800 North, Suite 218, Salt Lake City, Utah 84103, USA

Abstract

We derived a simple energy release rate analysis for the microbond specimen that includes energy released due to thermal stresses. By assuming that the droplet debonds from the fiber when the energy released from interfacial crack growth exceeds the fracture toughness of the interface, we predicted debond force as a function of droplet length and diameter. This fracture mechanics model of the microbond specimens agrees better with experimental results than the commonly used *average* shear stress failure criterion.

Introduction

Many researchers have used model single fiber composites to study the fiber/matrix interface. A recently developed single fiber technique, the microbond test, has been shown to be a reproducible and relatively simple test method [1–7]. Figure 1A shows a schematic view of the microbond test. The fiber is threaded between a vice or two knife edges and pulled. The knife edges contact the matrix droplet eventually shearing off the droplet when the load on the fiber gets to the debond load for the specimen. The experimental data are the debond load and the specimen geometry (*i.e.*, fiber radius, droplet diameter, and droplet length). Our goal was to develop a fracture mechanics method for interpreting experimental microbond test data.

The most widely used approach for analyzing failure in microbond specimens is to assume that the droplet shears off the fiber when the *average* shear stress at the interface, $\langle\tau_{rz}(\xi = 1)\rangle$, reaches the interfacial shear strength, τ_{ic} . By integrating the equations of stress equilibrium it is possible to derive an exact relation between $\langle\tau_{rz}(\xi = 1)\rangle$ and fiber force, F :

$$\langle\tau_{rz}(\xi = 1)\rangle = \frac{F}{2\pi r_1 l} \quad (1)$$

where r_1 is the fiber radius and l is the droplet length. The force, F_d , or stress, $\sigma_d = -\sigma_m V_2/V_1$, in the fiber at the instant of debonding is thus predicted to be linear in droplet length or aspect ratio (ρ):

$$F_d = 2\pi r_1 l \tau_{ic} \quad \text{or} \quad \sigma_d = 4\tau_{ic} \rho \quad (2)$$

There are two problems with Eq. (2). First, it does not agree with experimental data over a wide range of droplet lengths. Results in this paper and in other publications [2, 5, 8] show that debond stress is not linear in ρ , but rather levels off at large ρ . Second, despite that fact that Eq. (1) is an exact expression of stress equilibrium, the assumption that average shear stress determines failure is unrealistic. A variational stress analysis [9, 10] or a finite element analysis [11] shows that the shear stress is nonuniform and that there is a significant radial tensile stress concentration at the point where the fiber enters the droplet. It is probably incorrect to ignore these features of the stress state and attribute failure only to the level of average interfacial shear stress.

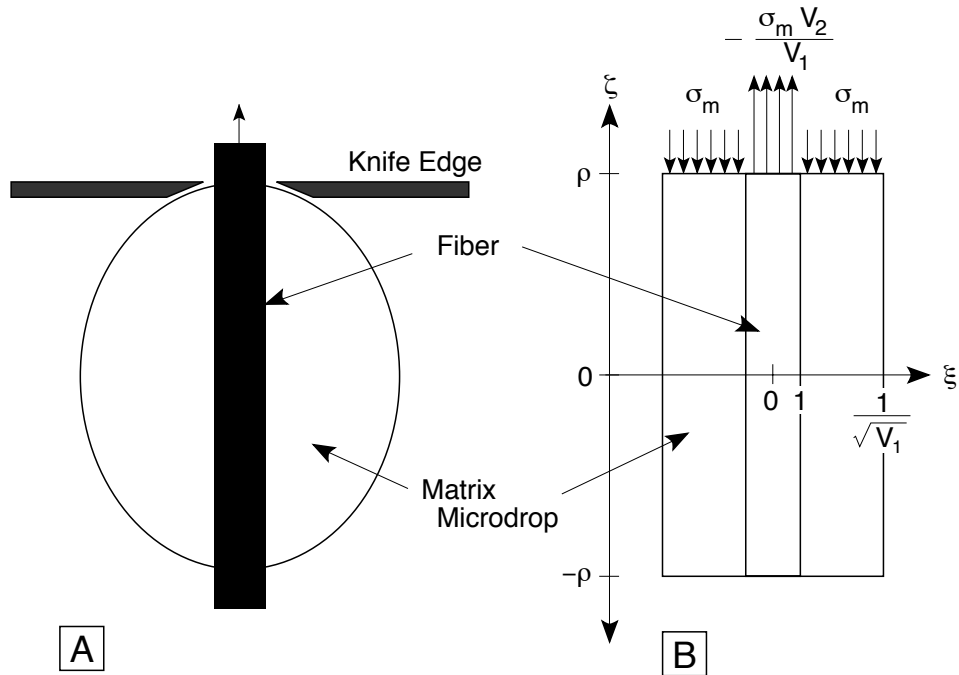


Figure 1: A microbond specimen of dimensionless length 2ρ , showing the actual specimen, (A), and an idealized cylindrical model, (B), under test loading conditions. σ_m is the stress applied to the droplet during the test. ξ and ζ represent dimensionless radial and axial coordinates, respectively. The stresses on the top of the fiber and matrix are balanced. In other words, the net axial stress on any cross-section ($\sigma_0 = V_1\sigma_f + V_2\sigma_m$) is assumed to be zero or the background fiber stress is assumed to be negligible.

In this paper we discuss a fracture mechanics method where debonding is predicted based on the energy release rate for initiation of an interfacial crack. The highest interfacial stresses are at the point where the matrix is contacted by the microvise [9, 10]. It is therefore logical to assume that debonding will be caused by initiation of an interfacial crack at that location. This assumption agrees with experimental observations of microbond failures [12]. We present a simple method for calculating the energy release rate for initiation of an interfacial crack — G_i . By assuming that specimen failure occurs when G_i reaches the critical energy release rate for the interface, or the interfacial toughness, G_{ic} , we can predict σ_d as a function of droplet length. The predictions were compared to our own experimental results and to some literature experimental results.

Materials and Methods

Microbond specimens were prepared by placing a microscopic droplet of epoxy resin (diameter 20-200 μm) on a fiber and curing the droplet by following vendor-recommended procedures. Sample measurements of droplet diameter and droplet length were recorded for each specimen. The specimens were then placed in a microbond jig and the fibers were translated upward at a steady rate while the droplet was held in place by means of two microvise grips (see Fig. 1). The knife edges were kept as close as possible to the fiber without actually touching. The droplet was continually observed through a telescope to confirm a clean and complete debond event. During the debond procedure, the load on the fiber was recorded by computer.

The matrix material was Epon 828 which consists of a diglycidylether of bisphenol A (DGEBA) liquid epoxy resin, and meta-phenylenediamine (MPDA), an amine curing agent. DGEBA

Table I: Mechanical and thermal properties of the fibers and matrix used in this paper and linear fitting parameters for predicting droplet diameter as a function of length. The transverse and shear properties of Kevlar[®] 49 aramid fibers are difficult to determine. The numbers in this table are estimates.

Property	E-Glass	Kevlar [®] 49	Epon 828
Diameter ($2r_1$) (μm)	21	11.7	
Tensile Modulus (E_A or E_m) (GPa)	75	130	3.3
Transverse Modulus (E_T) (GPa)	75	10	
Axial Shear Modulus (G_A or G_m) (GPa)	32	15	1.23
Axial Poisson's Ratio (ν_A or ν_m)	0.17	0.2	0.35
Transverse Poisson's Ratio (ν_T)	0.17	0.35	
Axial CTE (α_A or α_m) (ppm/ $^{\circ}\text{C}$)	5	-2	48
Transverse CTE (α_T) (ppm/ $^{\circ}\text{C}$)	5	60	
Diameter <i>vs.</i> Length Slope (A)	0.878	0.943	
Diameter <i>vs.</i> Length Intercept (B) (μm)	-40.6	-33.2	

and MPDA were purchased from Shell Chemical Company and Aldrich Chemical Company, respectively. The epoxy droplets were cured on the fibers at 75°C for 2 hours and at 125°C for 3 hours. Our experiments used E-glass fibers (obtained from Owens-Corning Fiberglass in Toledo, Ohio) with a diameter of $21\ \mu\text{m}$. The E-glass fibers were used in their as-received state and care was taken not to contaminate the fiber surfaces with oils, dust, or solvents. The literature data we analyzed used Kevlar[®] 49 aramid fibers (obtained from DuPont in Wilmington, Delaware). Table I summarizes some physical properties of these fibers and the Epon 828 matrix; the table also gives the nomenclature used to denote fiber and matrix mechanical properties.

Simple Fracture Mechanics Analysis

For a crack propagation analysis, we must consider a microbond specimen with an interfacial crack. Figure 2 shows an idealized microbond specimen with a crack of length a . We introduce a dimensionless coordinate system. The dimensionless coordinate in the radial direction is $\xi = x/r_1$. The dimensionless coordinate in the axial direction is $\zeta = z/r_1$. In the ξ - ζ coordinate system, the droplet length is 2ρ (or aspect ratio is ρ) and the crack length is 2δ where $\delta = a/2r_1$. For analysis we divide the specimen into two regions—region I is the region within the interfacial crack and region II is the region with an intact interface. Our first step is to find the stresses and strain energies in each region. We then use these results to calculate the energy release rate for growth of the interfacial crack.

Stresses and Strain Energies

Because the interfacial radial stress is tensile before crack formation [9, 10], we assume the crack in Fig. 2 opens and that the crack surfaces are stress free. We further assume that the axial stresses in region I are independent of the radial coordinate. The only possible stress state in region I in which σ_{zz} is independent of r is simple uniaxial tension. The axial stresses in the fiber and matrix are therefore

$$\sigma_{zz,1} = -\frac{\sigma_m V_2}{V_1} \quad \text{and} \quad \sigma_{zz,2} = \sigma_m \quad (3)$$

where subscripts 1 and 2 denote the fiber and matrix, respectively, and V_1 and V_2 are volume fractions. All other stresses in region I are zero. By volume integration, the total strain energy

special case. Thus, from Ref. [9]:

$$\begin{aligned} \sigma_{zz,1}^{(\infty)} &= \psi_\infty & \sigma_{rr,1}^{(\infty)} &= \sigma_\infty & \sigma_{\theta\theta,1}^{(\infty)} &= \sigma_\infty \\ \sigma_{zz,1}^{(\infty)} &= -\frac{V_1}{V_2}\psi_\infty & \sigma_{rr,1}^{(\infty)} &= -\frac{V_1\sigma_\infty}{V_2}\left(1 - \frac{1}{\xi^2 V_1}\right) & \sigma_{\theta\theta,1}^{(\infty)} &= -\frac{V_1\sigma_\infty}{V_2}\left(1 + \frac{1}{\xi^2 V_1}\right) \end{aligned} \quad (7)$$

where ψ_∞ is the far-field stress in the fibers (denoted as ψ_0 in Ref. [9]), σ_∞ is the far field radial stress at the interface (see Ref. [9] for an expression for σ_∞), and the shear stresses are all zero. Combining these stresses with the perturbation stresses, the total strain energy in region II can be integrated to give

$$U_{II}(\rho - \delta) = 2\pi r_1^3(\rho - \delta) \frac{D_3^2 \Delta T^2}{C_{33}} + U_p \quad (8)$$

where U_p is the energy due to the perturbation stresses and

$$C_{33} = \frac{1}{2} \left(\frac{1}{E_A} + \frac{V_1}{V_2 E_m} \right) - \frac{V_2 A_3^2}{V_1 A_0} \quad (9)$$

$$D_3 = \frac{1}{2} (\alpha_A - \alpha_m) - \frac{V_2 A_3}{V_1 A_0} (\alpha_T - \alpha_m) \quad (10)$$

$$A_0 = \frac{V_2(1 - \nu_T)}{V_1 E_T} + \frac{1 - \nu_m}{E_m} + \frac{1 + \nu_m}{V_1 E_m} \quad (11)$$

$$A_3 = - \left(\frac{\nu_A}{E_A} + \frac{V_1 \nu_m}{V_2 E_m} \right) \quad (12)$$

The strain energy due to the far-field stresses is a special case of Eq. (21) in Ref. [9] except that a typo has been corrected giving r_1^3 above instead of the r_1^2 in Ref. [9].

Energy Release Rate Analysis

The total energy release rate associated with growth of the crack in Fig. 2 is [13]

$$G_i = \frac{\partial W}{\partial A} - \frac{\partial U}{\partial A} = \frac{\partial W}{\partial A} - \frac{\partial U_I(\delta)}{\partial A} - \frac{\partial U_{II}(\rho - \delta)}{\partial A} \quad (13)$$

where W is external work, U is total specimen strain energy, and $A = 2\pi r_1 a = 4\pi r_1^2 \delta$ is total crack area. We consider the knife edges as fixed. When the debond extends, the only external work is the work done by the fiber stresses which is expended through the distance $u_f - u_m$ (see Fig. 2). Thus,

$$\frac{\partial W}{\partial A} = \frac{1}{4\pi r_1^2} \frac{\partial W}{\partial \delta} = \frac{\sigma_d}{4} \frac{\partial (u_f - u_m)}{\partial \delta} \quad (14)$$

By integrating the strains in region I (including thermal strains), the relevant displacement difference is

$$u_f - u_m = 4\delta r_1 (D_{3s} \Delta T + C_{33s} \sigma_d) \quad (15)$$

where

$$D_{3s} = \frac{1}{2} (\alpha_A - \alpha_m) \quad (16)$$

Substituting Eqs. (15) and (14) into Eq. (13) gives

$$G_i(\delta) = \frac{r_1}{2} \left[C_{33s} \sigma_d^2 + 2D_{3s} \sigma_d \Delta T - \frac{1}{2\pi r_1^3} \frac{\partial U_{II}(\rho - \delta)}{\partial \delta} \right] \quad (17)$$

In differentiating U_{II} with respect to δ , we note that the perturbation strain energy will be a constant as long as $\delta \ll \rho$ or as long as the crack tip is in the initial stages of growth and far away from the end of the droplet. The perturbation strain energy comes from a stress

singularity that propagates along with the crack tip, but does not change in intensity. Because of this simplification, the only energy released from region II is the release of far-field strain energy. This energy is released because region II gets smaller as the crack gets longer. The total strain energy release rate, which is now independent of δ becomes

$$G_i(\delta) = \frac{r_1}{2} \left[C_{33s} \sigma_d^2 + 2D_{3s} \sigma_d \Delta T + \frac{D_3^2 \Delta T^2}{C_{33}} \right] \quad (18)$$

In Ref. [10], we compared Eq. (18) to two analytical models that included the perturbation stresses and to finite element analysis. Equation (18) agrees well with both analytical models for all droplet aspect ratios corresponding to typical experimental conditions. Equation (18) also agrees within 20% with finite element calculations. Because of the difficulty in numerically analyzing stresses at interfacial crack tips, however, it was uncertain whether or not the finite element analyses had converged to the correct energy release rate.

Equation (18) gives total energy release rate. The finite element analysis [10], however, can be partitioned into mode I and mode II energy release rates. This partitioning reveals that initiation of debonding is pure mode I fracture. This calculation is contrary to the simplistic view of the microbond test as shearing off the droplet and therefore being a mode II fracture. The explanation is that before crack initiation there is a large tensile radial stress at $\zeta = +\rho$ and boundary conditions dictate that interfacial shear stress is zero [9, 10]. This stress state leads to mode I fracture. As the crack grows, the stress state changes and finite element analysis shows that the amount of mode II deformation increases. If debonding is controlled by the initiation of the interfacial crack, however, the microbond test should be considered as measuring the *tensile* or mode I failure properties of the interface and not the interfacial *shear* strength or mode II failure properties.

To predict debonding, we assumed a microbond specimen debonds when the energy release rate for crack initiation is equal to the interfacial fracture toughness, Solving Eq. (18) and taking the positive root gives

$$\sigma_d(\rho) = -\frac{D_{3s} \Delta T}{C_{33s}} + \sqrt{\frac{2G_{ic}}{r_1 C_{33s}} + \frac{\Delta T^2}{C_{33s}} \left(\frac{D_{3s}^2}{C_{33s}} - \frac{D_3^2}{C_{33}} \right)} \quad (19)$$

In the absence of thermal loads, this expressions simplifies farther to

$$\sigma_d(\rho, \Delta T = 0) = \sqrt{\frac{2G_{ic}}{r_1 C_{33s}}} \quad (20)$$

Results

To generate a representative set of data, several fiber types were tested and the microdrop size (length and diameter) was varied among the samples. Each sample's droplet length and diameter were recorded prior to debonding. Only axisymmetric droplets were tested. The debond event was monitored through a telescope positioned near the test sample, and three possible outcomes were noted; partial debond, droplet shatter, and complete debond. Only the results from complete debonds were used (for more details see Ref. [8]). Although there was much scatter in the individual data points, a simple smoothing routine can be applied to the data points. We smoothed the data by averaging the debond force data over 20 μm increments of length. The smoothed debond force data as a function of droplet length are plotted in Figs. 4 and 5 for both our 21 μm diameter E-glass fibers and Tesoro's Kevlar 49[®] data [2]. The error

bars on the experimental data points are the standard deviation of the raw data points within the 20 μm range of smoothed data.

Equation (19) gives debond stress in terms of mechanical properties of the fiber and the matrix and of the geometry of the specimen. Unlike Eq. (2), Eq. (19) is not merely a function of droplet length. It also depends on the fiber and matrix volume fractions. To fit experimental results of debond force as a function of droplet length, it is clearly insufficient to follow the standard practice of recording only droplet length and debond force [1–7]. To do an energy release rate analysis, we must also record V_1 as a function of droplet length.

We calculated V_1 and V_2 from the measured droplet diameter (D) and length (l). The droplet/fiber region of the specimen was assumed to be a ellipsoid of revolution with total volume:

$$V = \frac{4\pi}{3} \left(\frac{D}{2}\right)^2 \left(\frac{l}{2}\right) \quad (21)$$

The volume fraction of the fiber is then

$$V_1 = \frac{\pi r_1^2 l}{V} = 1.5 \left(\frac{r_1}{r_2}\right)^2 \quad (22)$$

where r_2 is the radius of the droplet. We recorded droplet diameters for each specimen, but, for theoretical predictions it is preferable to have a relation between diameter and length. A plot of droplet diameter as a function length for one of the systems tested (a 21 μm diameter E-glass fiber with EPON 828 droplets) is shown in Fig. 3. These data were fit to a line

$$D(l) = Al + B \quad (23)$$

As seen in Fig. 3, the fit is excellent over the entire range of experimental results. The linear relation, however, is only expected to be valid when $D \gg 2r_1$, because it is impossible for the droplet diameter to be less than the fiber diameter. In other words $D(l)$ will not continue to follow the line as l decreases, but instead will level off at $D \approx 2r_1$. There is a some indication of $D(l)$ leveling off at the lowest l values in Fig. 3. As long as we restrict analysis to droplets within the range of experimental droplets, the linear relation provides an accurate measure of $D(l)$. A consequence of not being able to extrapolate $D(l)$ to small l is that our theoretical debond-force curves do not pass through the origin. If necessary, this artifact could be corrected by using a more complicated form of $D(l)$ that works for all l . The fitting results for linear $D(l)$ for both material systems analyzed in this paper are given in Table I.

Experimental results and theoretical predictions for debonding EPON 828 droplets off 21 μm E-glass fibers are shown in Fig. 4. The solid line gives a theoretical prediction with an interfacial toughness of $G_{ic} = 222 \text{ J/m}^2$. Based on the processing conditions, we assumed the thermal load was $\Delta T \approx 100^\circ\text{C}$. The thermal stresses contributed about 10% of the total energy release rate. Although we have no independent measure of interfacial toughness, we note that a toughness value of 222 J/m^2 is in line with physical expectations for crack growth in epoxy systems.

Experimental results and theoretical predictions for debonding EPON 828 droplets off Kevlar[®] 49 aramid fibers are shown in Fig. 5. The experimental results in Fig. 5 are from Ref. [2]. Because that paper did not give the droplet diameter as a function of droplet length, we did some of our own experiments with Epon 828 droplets on Kevlar[®] 49 aramid fibers. The linear fit between $D(l)$ and l (see Table I) from our data was used to analyze the data in Fig. 5. The interfacial toughness used to generate the fit to experimental data was $G_{ic} = 106 \text{ J/m}^2$. Thus the interface between EPON 828 and Kevlar[®] 49 aramid fibers is less tough than the interface between EPON 828 and E-glass fibers.

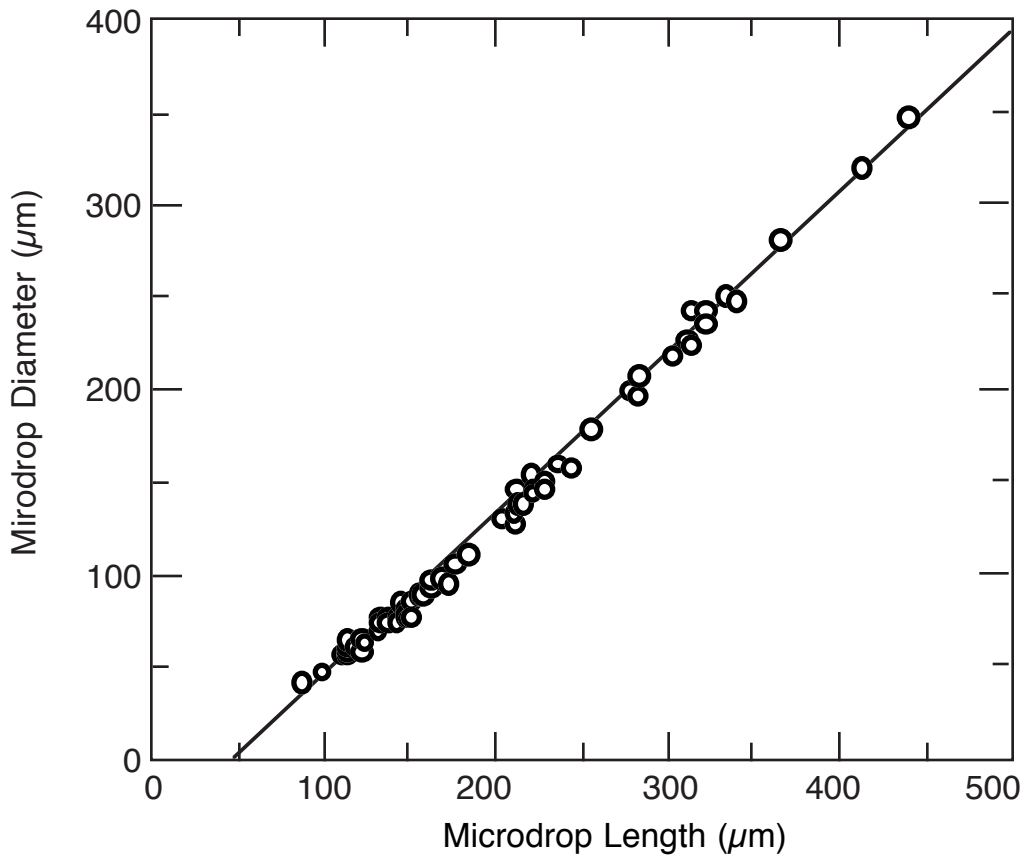


Figure 3: Plot of droplet diameter as a function of droplet length data for EPON 828 droplets on E-glass fibers of diameter $21 \mu\text{m}$. The solid line is the best linear fit to the experimental data.

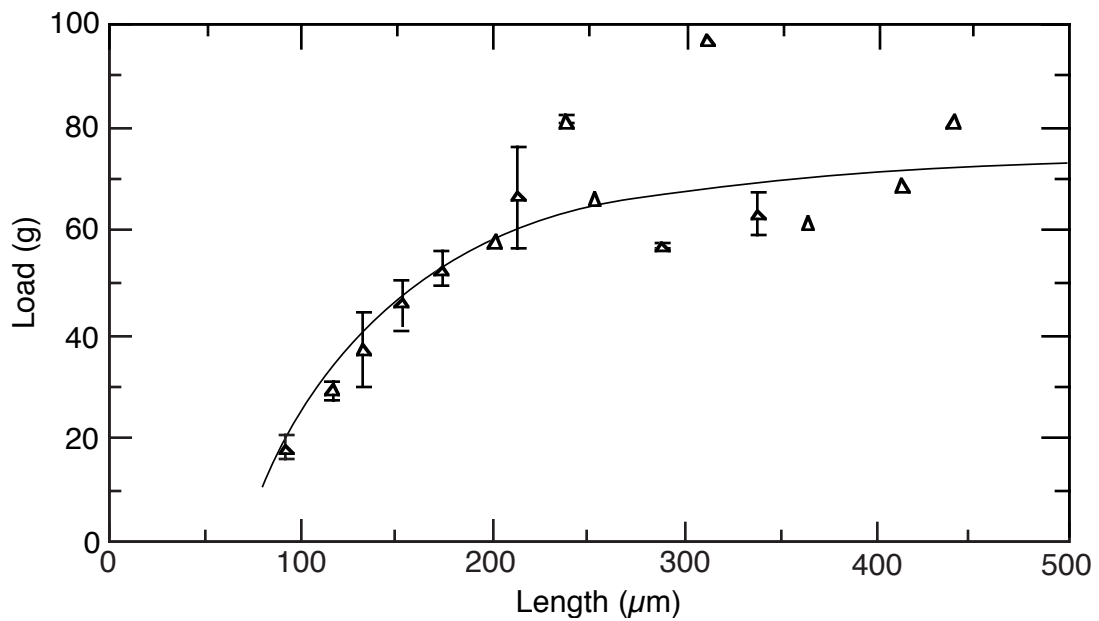


Figure 4: Plot of debond load versus microdrop length for debonding of EPON 828 droplets off $21 \mu\text{m}$ diameter E-glass fibers. The smooth line is a theoretical fit to the experiments using the energy release rate theory and a critical value of $G_{ic} = 222 \text{ J/m}^2$.

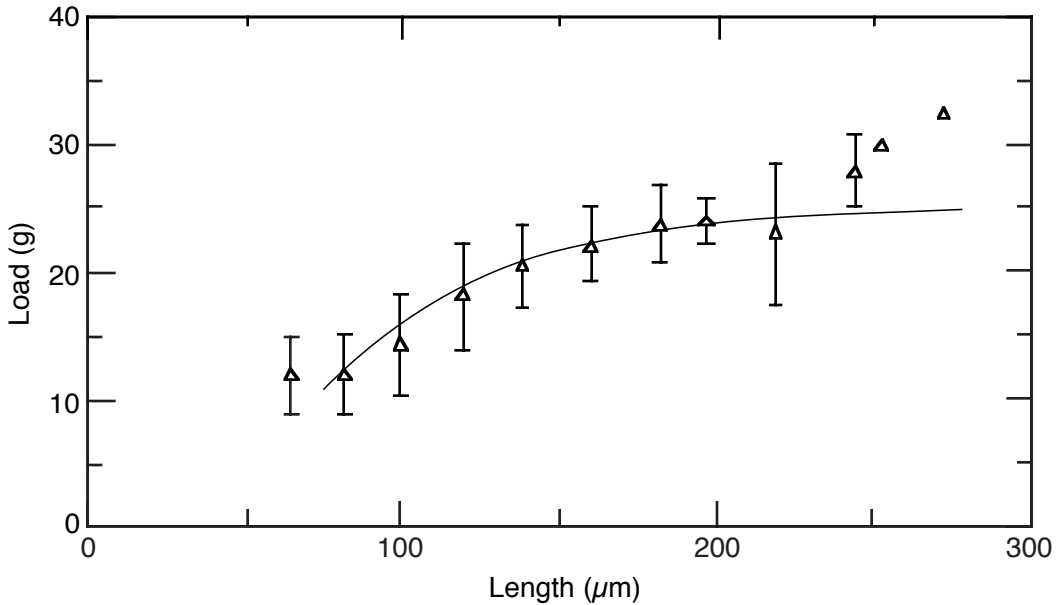


Figure 5: Plot of debond load versus microdrop length for debonding of EPON 828 droplets off Kevlar® 49 aramid fibers. The smooth line is a theoretical fit to the experiments using the energy release rate theory and a critical value of $G_{ic} = 106 \text{ J/m}^2$.

Discussion and Conclusions

The simple energy release rate analysis agrees well with both experimental data sets presented above. The process of fitting the analysis to experimental results allows one to measure the interfacial toughness, G_{ic} . This toughness should be interpreted as a mode I toughness of the interface. In conducting an energy release rate analysis, we noted that it is insufficient to record only debond force and droplet length. The energy release rate equation also depends on fiber volume fraction (V_1). This volume fraction can be measured by additionally recording droplet diameter. We thus recommend that future microbond experiments measure debond force as a function of droplet length *and* droplet diameter.

Recent scanning wettability studies of fibers after the debonding process show that the fracture process is rarely a pure interfacial fracture [6, 7]. Instead it is common to see cohesive failure within the fiber, in which case a small amount of the surface of the fiber is removed, or cohesive failure within the matrix, in which case a small amount of matrix remains on the fiber. These observations might seem to invalidate the analysis of this paper which assumes an interfacial fracture, but actually they do not. Consider analyzing experiments which all fail by the type of matrix cohesive fracture observed in Ref. [6]. The matrix left on the fiber affects the stress analysis in region I (see Fig. 2). The fiber part of region I should be slightly larger and have different mechanical properties while the matrix part should be slightly smaller. The amount of matrix left on the fiber, however, is exceedingly small; it is beyond the resolution of scanning electron microscopy [6]. Thus the effect of the matrix left on the fiber on the strain energy in region I will be negligible. The failure mode also has no effect on the strain energy in region II because the interface in that region is still intact. We finally conclude that the energy release rate calculated in this paper is valid for any failure mode as long as the amount of matrix left on the fiber during matrix cohesive failure or the amount of fiber removed during fiber cohesive failure is small.

Although our energy release rate and the method for determining G_{ic} are valid, the interpre-

tation of G_{ic} is profoundly affected by failure mode. G_{ic} is only an *interfacial* toughness when the failure mode is at the interface. Matrix failures and fiber failures require reinterpreting G_{ic} as either a matrix cohesive toughness or a fiber cohesive toughness. Microbond tests should therefore always be supported by careful observation of the failure process by techniques such as scanning wettability [6].

Acknowledgements

This work was supported by a grant from the Mechanics of Materials program at NSF (CMS-9401772), by a contract from NASA Langley Research Center (NAS1-18833) monitored by Dr. John Crews, and by a gift from the Fibers Department of E. I. duPont deNemours & Company monitored by Dr. Alan R. Wedgewood. Additionally, R. J. Scheer was supported by an NSF graduate fellowship and a University of Utah research fellowship

References

1. B. Miller, P. Muri, and L. Rebenfeld, "A Microbond Method for Determination of the Shear Strength of a Fiber/Resin Interface," *Comp. Sci. & Tech.*, **28**, 1987, pp. 17–32.
2. G. C. Tesoro, R. Benrashid, L. Rebenfeld, and U. Gaur, *International Symposium on Polymers for Advanced Technologies*, Jerusalem, Israel, August 17-21, 1987, pp. 773–791.
3. R. A. Haaksma and M. J. Cehelnik, "A Critical Evaluation of the Use of the Microbond Method for Determination of Composite Interfacial Properties," *Mat. Res. Soc. Symp. Proc.*, **170**, 1990, pp. 71–76.
4. V. Rao, P. Herrera-Franco, A. D. Ozzello, and L. T. Drzal, "A Direct Comparison of the Fragmentation Test and the Microbond Pull-Out Test for Determining the Interfacial Shear Strength," *J. Adhesion*, **34**, 1991, pp. 65–77.
5. H. D. Wagner, H. E. Gallis, and E. Wiesel, "Study of the Interface in Kevlar 49/Epoxy Composite By Means of the Microbond and the Fragmentation Tests: Effect of Materials and Testing Variable," *J. Mat. Sci.*, **28**, 1993, pp. 2238–2244.
6. C. T. Chou, U. Gaur, and B. Miller, "Fracture Mechanisms During Fiber Pull-Out for Carbon-Fiber-Reinforced Thermosetting Composites," *Comp. Sci. & Tech.*, **48**, 1993, pp. 307–316.
7. C. T. Chou, U. Gaur, and B. Miller, "Evaluation of Fracture Surfaces in Carbon Fiber/Epoxy Composites," *J. Adhesion*, **40**, 1993, pp. 245–256.
8. R. J. Scheer, "Application of a Variational Mechanics Stress Analysis and Energy Based Failure Criteria to the Microdrop Debond Test for Evaluation of the Adhesion Quality of Several Fiber-Matrix Systems," PhD Thesis, University of Utah, 1993.
9. R. J. Scheer and J. A. Nairn, "Variational Mechanics Analysis of the Stresses and Failure in Microdrop Debond Specimens," *Composites Engineering*, **2**, 1992, pp. 641–654.
10. R. J. Scheer and J. A. Nairn, "A Comparison of Several Fracture Mechanics Methods for Measuring the Interfacial Toughness with Microbond Tests," *J. Adhesion*, submitted, 1994.
11. R. J. Day and M. Marquez, "The Micromechanics of the Microbond Test," in *International Phenomena in Composite Materials*, eds., I. Verpoest and F. R. Jones, Butterworth-Heinemann Ltd., Oxford, England, 1991, pp. 65–68.
12. L. S. Penn and S. M. Lee, "Interpretation of Experimental Results in the Single Pull-Out Filament Test," *J. Comp. Tech. & Res.*, **11**, 1989, pp. 23–30.
13. J. G. Williams, *Fracture Mechanics of Polymers*, John Wiley & Sons, New York, 1984, p. 24.